ELSEVIER

Journal of Alloys and Compounds 260 (1997) 265–270

Journal of ALLOYS AND COMPOUNDS

$ZrV_{1.5}Ni_{1.5}$ as electrode material in nickel–metal hydride batteries An in situ scanning tunnelling microscopy investigation

Daniel Chartouni*, Andreas Züttel, Christoph Nützenadel, Louis Schlapbach

University of Fribourg, Institute of Physics, Pérolles, CH-1700 Fribourg, Switzerland

Received 7 March 1997; received in revised form 20 March 1997

Abstract

We have investigated the alloy $ZrV_{1.5}Ni_{1.5}$ by means of scanning electron microscopy (SEM) with electron probe X-ray microanalysis (EPMA), X-ray diffraction (XRD), in situ STM (scanning tunnelling microscopy in an electrolyte under controlled electrochemical potential) and electrochemical charge discharge measurements. By means of EPMA we found that the alloy is composed of three different crystallographic phases. The main phase (≈75 vol.%) is $ZrV_{0.81}Ni_{1.47}$, the second phase (≈20 vol.%) is $V_{92}Ni_8$ and the third (≈5 vol.%) is a ZrNi based phase. Using in situ STM we investigated the different corrosion behaviour of the phases. At a potential of −600 mV versus the Hg/HgO reference electrode we observed the corrosion of the vanadium rich phase while the other two phases passivated. © 1997 Elsevier Science S.A.

Keywords: Metal hydrides; Electrode; $ZrV_{1.5}Ni_{1.5}$; In situ scanning tunnelling microscopy

1. Introduction

In commercial nickel–metal hydride batteries AB_5 or AB_2 type alloys are used as negative electrode material [1,2]. The discharge capacity of the electrodes is generally about 250–320 $mAh \cdot g^{-1}$ of active material [3,4]. There is an urgent demand for much higher capacities in rechargeable batteries.

Previous investigations of Laves phase AB_2 type metal hydride electrodes have shown that the presence of a small quantity of a second phase can improve the hydriding characteristics [5,6]. For example, the two phase alloy $Zr(V_{0.25}Ni_{0.75})_2$ is composed of a C15 Laves phase (main phase) and a Zr_7Ni_{10} secondary phase [7]. The rate capability for the two phase alloy was found to be superior than that of each of the separate phases [5]. This interesting effect has also been studied in the system containing $Zr(Cr_{0.4}Ni_{0.6})_2$ as the main phase and Zr_7Ni_{10} as secondary phase [6]. In this case the measured electrochemical discharge capacity of the two phase alloy is higher than that of each phase, separately.

As a third example, $TiV_3Ni_{0.56}$ was found to contain two phases, a TiV based main phase and a TiNi based secondary phase [8]. The authors concluded that acting as a catalyst and/or a current collector, the secondary phase would enhance the electrochemical reaction of the TiV based primary phase. Further investigation of this alloy showed that during cycling Ti and V of the secondary phase were dissolved into the electrolyte limiting the cycle life of the electrode [9].

The investigation of multiphase alloys requires a method in which electrical properties and topographical structures of the surface [10,11] can be measured in situ. In situ STM offers the possibility of time resolved imaging of the electrode topography with high spatial resolution [12–14].

In this paper we present an investigation of the corrosion behaviour of this multiphase alloy by means of XRD, SEM and in situ STM.

2. Experimental

2.1. Sample preparation and ex situ measurements

The alloy $ZrV_{1.5}Ni_{1.5}$ was prepared by r.f. levitation melting. The appropriate amount of elements (Zr 99.95% from Johnson Matthey, UK, and V 99.8% and Ni 99.7% from Goodfellow, UK) were melted in a water-cooled copper crucible inside a quartz tube in a vacuum of 10^{-6} mbar. Upon 4 min at 1400 °C the pellet was cooled to room temperature. The pellet was remelted once again for 4 min at 1400 °C and rapidly cooled to room temperature

*Corresponding author. Tel.: (41-26) 300-9086; fax: (41-26) 300-9747; e-mail: daniel.chartouni@unifr.ch

PII S0925-8388(97)00167-9

(within seconds). The sample was cracked in air and some pieces of about 4 mm in diameter were mounted in epoxy resin and polished with diamond paste to 1/4 μm and finely polished on velvet. The polished samples were used for scanning electron microscopy (SEM) and in situ STM investigations.

The remaining part of the alloy (about 3 g) was ground to an average grain size of about 100 μm and pulverized by cycling it several times with hydrogen gas (20 bar). The powder material was used for XRD and electrochemical measurements.

X-Ray diffraction was performed using Cu Kα radiation. A maximum count rate of approximately 2200 counts was found for the main peak in the spectrum (2.2% error in the count rate) and the angular resolution was $2\Theta=0.3°$ (FWHM).

The polished bulk sample was examined by SEM with electron probe X-ray microanalysis (EPMA) in order to determine the composition of each phase of the alloy. The electron beam acceleration voltage used was 17 kV and the beam current was 20 nA. The X-ray lines for quantitative analysis were V Kα, Ni Kα and Zr Lα.

2.2. Electrochemical measurements

For electrochemical cycling about 30 mg of alloy powder was mixed with 80 mg copper powder (Merck p.a.) and pressed into a pellet (d=7 mm, $5\cdot10^8$ Pa). The electrode was stored for 13 h in 6 M KOH at 80 °C. Then the electrode was electrochemically charge–discharge cycled in an open halfcell (in a 6 M KOH electrolyte at room temperature) using a computer-controlled current source. The nickel counter electrode was placed in a separate compartment of the cell. The cell was charged to 600 $mAh\cdot g^{-1}$ with a constant current of 30 $mA\cdot g^{-1}$. The discharge-current was also 30 $mA\cdot g^{-1}$ and the discharge-limit was set to −600 mV with respect to the Hg/HgO reference electrode. Capacity was calculated from the discharge time. The electrode was activated electrochemically and after 10 cycles the current was then set to 100 $mA\cdot g^{-1}$ (referred to as the normal discharge current).

The maximum discharge capacity was measured at intervals by imposing an additional discharge with a lower current (half of the normal discharge current). The discharge procedure was repeated 6 times and the sum of the capacities is referred to as the maximum discharge capacity. We assume that in this manner the hydrogen was completely desorbed, even for hydrides with slow kinetics.

2.3. In situ STM measurements

We adapted a commercial scanning tunnelling microscope (NanoScope III) to be used with an electrochemical cell [15]. This allowed in situ STM measurements of electrode materials during electrochemical cycling. The sample, the Hg/HgO reference electrode and the counter electrode (platinum wire) are connected to an external potentiostat/galvanostat.

The $Pt_{80}Ir_{20}$ tips have been made by etching using a melted mixture of NaOH and $NaNO_3$ [16]. The tip preparation procedure was described previously [15]. The tips were insulated with apiezon wax [17] in order to minimize the faradaic charge transfer currents. Our experiments have shown that the insulation is stable for several hours in concentrated 6 M KOH. It is necessary to change the tip during long time duration experiments. Visually relocating the new tip on the sample surface is difficult because of the optical distortion caused by the surface tension of the electrolyte. Therefore a special optical element was constructed which provides an internal view of the tip-sample interface from outside with an optical microscope.

The electrochemical tip potential for stable tunnelling conditions in 6 M KOH is between −950 and +100 mV versus the Hg/HgO reference electrode. The potential of the sample was set to −600 mV for three days. At this corrosive potential the metal hydride electrode is in a completely discharged state. Imaging of the electrode surface was then performed to observe the corrosion behaviour of the alloy. High bias voltages were used (up to 500 mV in the electrolyte).

3. Results and discussion

The maximum discharge capacity of the $ZrV_{1.5}Ni_{1.5}$ multiphase alloy was found to be 503 $mAh\cdot g^{-1}$ at 40 °C. During normal cycling with 100 $mA\cdot g^{-1}$ reversible capacities of 225 $mAh\cdot g^{-1}$ could be measured. The very high maximum discharge capacity of more than 500 $mAh\cdot g^{-1}$ could not be achieved with further maximum discharges. About 330 $mAh\cdot g^{-1}$ were discharged in subsequent cycles (Fig. 1). Between the very first maximum discharge (after five normal cycles) and the following maximum discharges a difference of 175 $mAh\cdot g^{-1}$ at 40 °C was measured. At 20 °C the same behaviour could be observed.

Fig. 2 shows a secondary electron image of the polished $ZrV_{1.5}Ni_{1.5}$ surface. The black phase is $V_{92}Ni_8$, the main phase (grey) is $Zr(V_{0.35}Ni_{0.65})_{2.28}$ and the remaining phase (white) is a ZrNi based phase with a composition of $Zr_{\approx 43}Ni_{\approx 57}$. The results of the EPMA and XRD measurements are summarized in Table 1. The ordered pattern of the vanadium rich phase has also been observed by Miyamura et al. [18] in a $Ti_{0.5}Zr_{0.5}Ni_{1.3}V_{0.7}Cr_{0.2}$ alloy. They suggest that the dendritic growth of the precipitation pattern from the melt might be because of the very high melting point of the vanadium (1900 °C).

The phase distribution in volume percent were roughly estimated from an SEM image to an accuracy of about ±5 vol.% (Table 1).

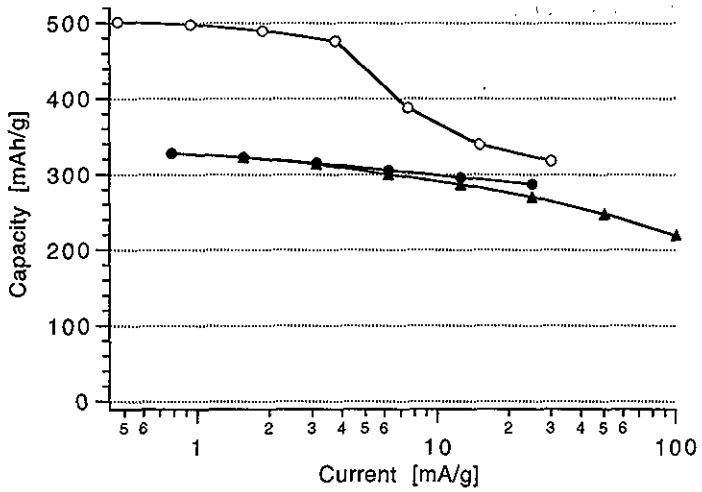

Fig. 1. Maximum discharge curves of the same $ZrV_{1.5}Ni_{1.5}$ electrode after 5 normal cycles (– ∘ –), after 9 (– · –) and after 14 normal cycles (– ▲ –) at 40 °C.

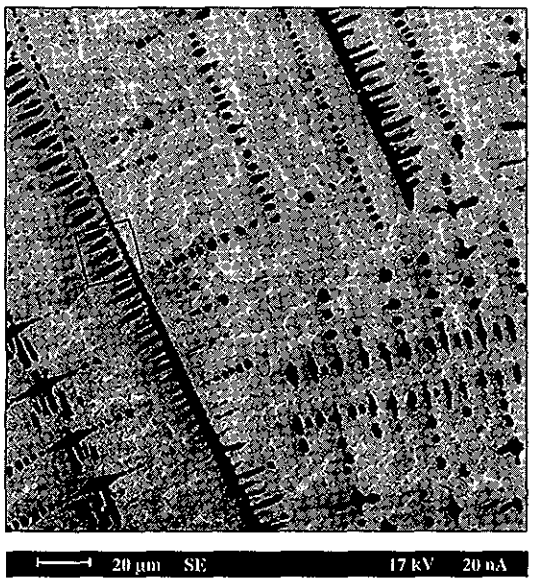

Fig. 2. Scanning secondary electron image of the polished $ZrV_{1.5}Ni_{1.5}$ sample. The black phase is $V_{92}Ni_8$, the gray phase is $Zr(V_{0.35}Ni_{0.65})_{2.28}$ (main phase) and the white phase is a ZrNi based phase. The region marked by the square was chosen for the in situ STM investigation (Fig. 5 and Fig. 6).

The square on Fig. 2 indicates the region on which in situ STM was performed (Fig. 5 and Fig. 6).

To exclude the possibility that the multiphase structure was created during the polishing process, characteristic X-ray maps were performed on fresh cleavage planes of single alloy particles. This was done by grinding the alloy to a maximum grain size of 150 µm and pressing the powder onto a soft indium pellet. This powder showed the same multiphase structure as the polished surface (Fig. 3).

The multiphase structure of the $ZrV_{1.5}Ni_{1.5}$ alloy can not be resolved in the measured XRD data. Only the structure of the main phase ($ZrV_{0.81}Ni_{1.47}$, identified by EPMA) can directly be perceived (Fig. 4, upper spectrum). However, the second phase ($V_{92}Ni_8$) has a cubic bcc structure with lattice parameter a=2.98 Å [19]. The main peak {110} in the XRD spectrum of $V_{92}Ni_8$ is at 2Θ=42.9°. This peak coincides with the {311} peak of the main phase in the alloy (Fig. 4). Therefore, only the two remaining {200} at 61.8° and {211} at 77.75° are visible in Fig. 4 (upper spectrum). Considering the intensities of these peaks and the number of electrons per volume of the different phases, we calculated a phase distribution 1:4 between this phase and the main phase of the alloy. The best fit of the recalculation of the spectrum for the vanadium rich phase

Table 1
Results of EPMA and XRD measurements

	Matrix phase	Second phase	Third phase
Volume of the alloy	≈75%	≈20%	≈5%
Measured composition	$ZrV_{0.81}Ni_{1.47}$	$Zr_{\sim 0}V_{\sim 92}Ni_{\sim 8}$	$Zr_{\sim 43}V_{\sim 0}Ni_{\sim 57}$
Probable composition	$Zr(V_{0.35}Ni_{0.65})_{2.28}$	$V_{92}Ni_8$	Zr_7Ni_{10}+ZrNi
Alloy type	Intermetallic compound	Solid solution	Mixture of two intermetallic comp. (?)
Structure	C15 Laves phase a=7.073 Å	bcc phase a=2.99 Å	Both orthorhombic

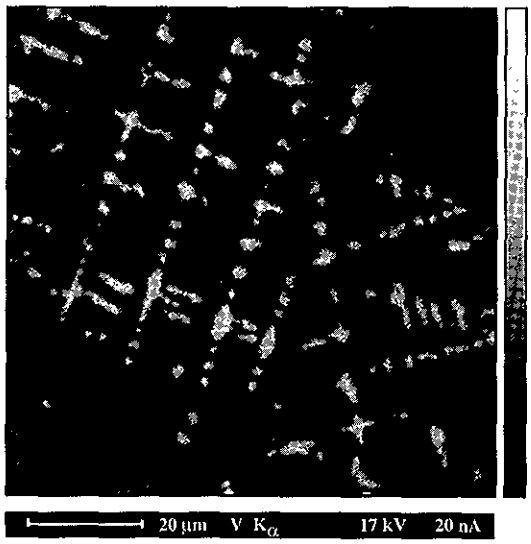

Fig. 3. Characteristic X-ray micrograph image of V Kα of a single $ZrV_{1.5}Ni_{1.5}$ grain pressed onto indium. Light regions have high vanadium concentrations, dark regions low vanadium concentration.

gave the parameter of a=2.99 Å [20]. The modelled spectrum is shown in Fig. 4 (lower spectrum) with the same intensity as in the measured spectrum. The fact that only 20 vol.% of the alloy is $V_{92}Ni_8$ and that the main peak of this phase coincides with the strongest peak of the main phase explains the apparent single phased nature of the measured spectrum. The small peaks at about 2Θ=40° are probably the main peaks of the third phase.

Fig. 5 shows an STM image of the topography of the polished sample in 6 M KOH at an electrochemical potential of −600 mV vs. Hg/HgO reference electrode. This is the region indicated with a square in Fig. 2. It can be seen, that the vanadium rich phase protrudes out of the surface. This is due to oxidation of the vanadium. The height of the periodic features is about 30 nm above the main phase.

Maintaining a potential of −600 mV, the sample was scanned again after 72 h. The vanadium rich phase has been dissolved (Fig. 6). The resulting holes are deeper than the limit of the tip movement (in this case 1 µm).

For the other two phases ($Zr(V_{0.35}Ni_{0.65})_{2.28}$ and $Zr_{\approx 43}Ni_{\approx 57}$) changes in the surface topography could not be observed. Zr–Ni alloy systems are known to form a solid ZrO_2 layer on the surface as a result of oxidation [21,22]. Apparently, this passivation layer protects these alloys from further corrosion. In solutions with a pH higher than 7 the solubility of ZrO_2 is about 7 orders of magnitude smaller than the solubility of V_2O_4 [23]. For a

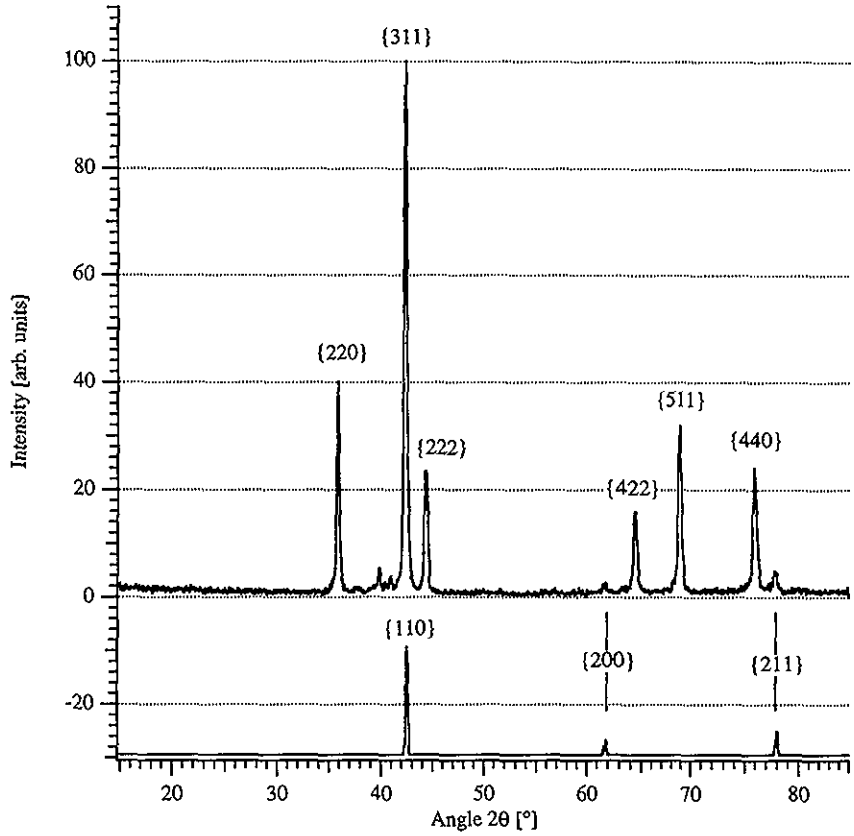

Fig. 4. Upper spectrum: measured X-ray diffraction pattern of $ZrV_{1.5}Ni_{1.5}$. The main phase has a cubic C15 Laves phase with lattice parameter a=7.073 Å. Lower spectrum: calculated X-ray diffraction pattern of the second phase $V_{92}N_8$ (see Table 1).

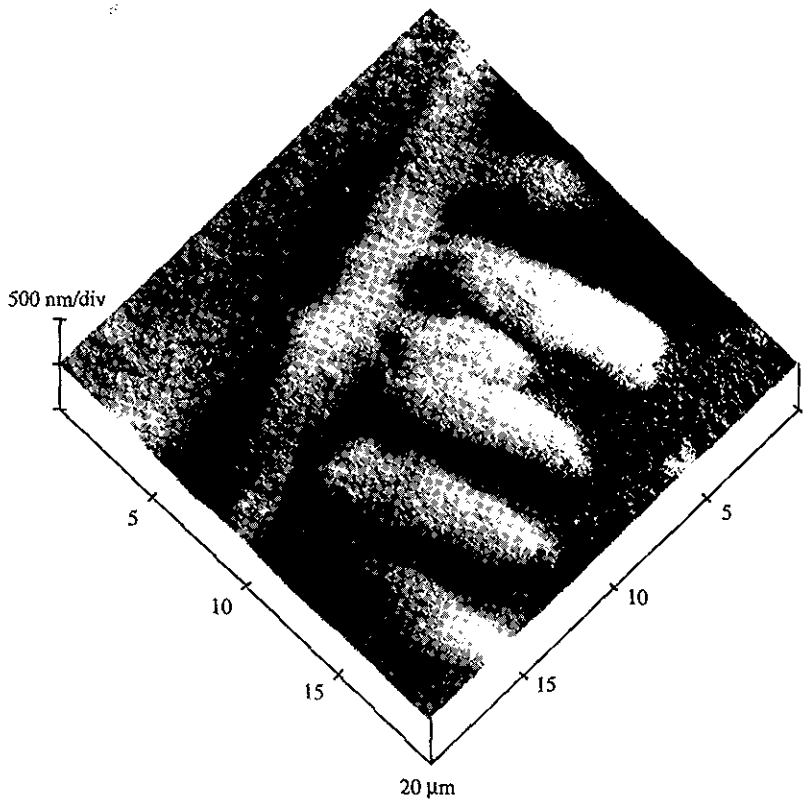

Fig. 5. In situ STM image of $ZrV_{1.5}Ni_{1.5}$ just after immersion in 6 M KOH at an electrochemical potential of $E = -600$ mV vs. Hg/HgO reference electrode. The periodic features are the vanadium rich phase which is oxidized at the surface.

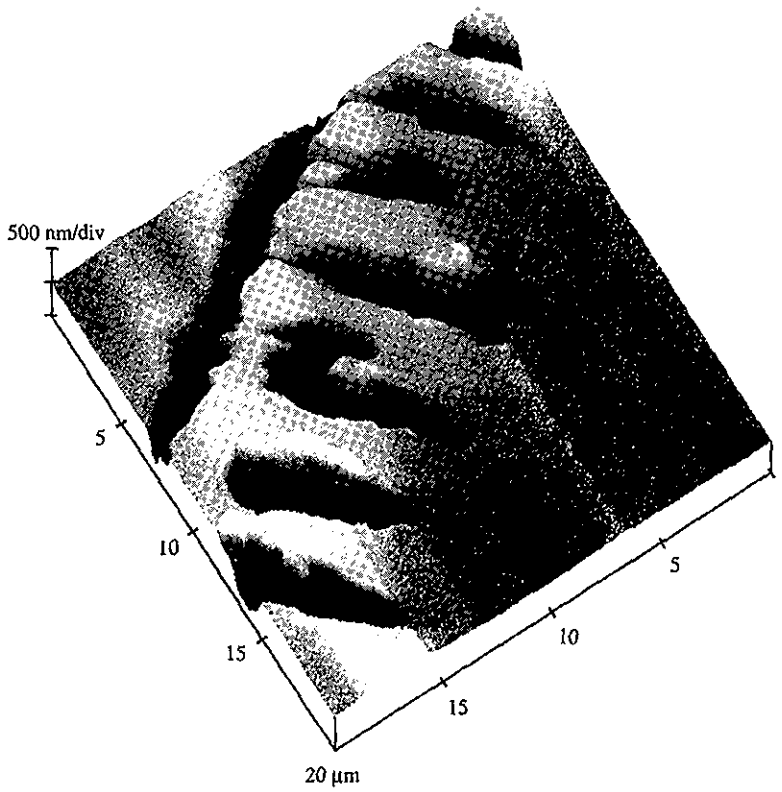

Fig. 6. Same region and same conditions as in Fig. 5 but after 72 h of immersion. The vanadium rich phase has dissolved into the electrolyte.

pH of 9, for example, the maximum amount of vanadium oxide which can be dissolved in the electrolyte is about 0.5 $mol \cdot l^{-1}$ compared with $0.5 \cdot 10^{-7}$ $mol \cdot l^{-1}$ for ZrO_2.

At the applied potential the surface of the $V_{92}Ni_8$ phase is oxidized to V_2O_4 and to $Ni(OH)_2$ [23]. The oxidation of the vanadium can be described by means of the following reaction:

$$2V + 4H_2O \rightarrow V_2O_4 + 4H_2.$$

The hydrogen can be absorbed into the metal hydride electrode and the vanadium oxide can easily be dissolved into the electrolyte:

$$V_2O_4 + OH^- \rightarrow HV_2O_5^-(solv.),$$

so that fresh surfaces of the vanadium rich phase are continuously available for oxidation. The hydrogen which was absorbed by the electrode can now be oxidized:

$$2H_{abs.} + 2OH^- \rightarrow 2H_2O + 2e^-.$$

This reaction, together with the reaction at the counter electrode

$$2e^- + 2H_2O \rightarrow 2OH^- + H_2\uparrow,$$

can lead to an apparent capacity due to corrosion of the vanadium rich phase. If we assume that 20 vol.% of the alloy is $V_{92}Ni_8$ we calculate an additional capacity of 354 $mAh \cdot g^{-1}$ alloy.

4. Conclusion

A $ZrV_{1.5}Ni_{1.5}$ electrode in 6 M KOH under a controlled electrochemical potential was observed over a period of 72 h by means of in situ STM. The three component phases in this alloy show a very different corrosion behaviour. While the two zirconium containing phases are more stable the vanadium rich secondary phase corrodes easily. The dissolution of the vanadium rich phase out of the alloy could be observed.

Acknowledgements

We wish to thank Prof. Siegenthaler and his group at the University of Bern for support and helpful discussions about in situ STM investigations. Furthermore, we thank Larryn Diamond from the Institute of Mineralogy and Petrography at the University in Bern for technical support on microprobe analysis and for the financial support by the Schweizerischer Nationalfonds (credit 21-26579.89) at the University in Bern.

References

[1] L. Schlapbach, F. Meli, A. Züttel, in: J.H. Westbrook, R.L. Fleischer (Eds.), Intermetallic Compounds, Vol. 2, John Wiley and Sons Ltd, 1994.
[2] J.J.G. Willems, Philips J. Res. 39(Suppl. 1) (1984) 1.
[3] T. Sakai, H. Yoshinaga, H. Miyamura, N. Kuriyama, H. Ishikava, J. Alloys Comp. 180 (1992) 37–54.
[4] D. Chartouni, A. Züttel, F. Meli, L. Schlapbach, J. Alloys Comp. 241 (1996) 160–166.
[5] A. Züttel, F. Meli, D. Chartouni, L. Schlapbach, F. Lichtenberg, B. Friedrich, J. Alloys Comp. 239 (1996) 175–182.
[6] J.M. Joubert, D. Sun, M. Latroche, A. Percheron-Guegan, Proceedings of the International Conference on Metal Hydrogen Systems, 1996, to be published in the Journal of Alloys and Compounds.
[7] A. Züttel, F. Meli, L. Schlapbach, J. Alloys Comp. 203 (1994) 235–241.
[8] M. Tsukahara, K. Takahashi, T. Mishima, T. Sakai, H. Miyamura, N. Kuriyama, I. Uehara, J. Alloys Comp. 226 (1995) 203–207.
[9] M. Tsukahara, K. Takahashi, T. Mishima, T. Sakai, H. Miyamura, N. Kuriyama, I. Uehara, J. Alloys Comp. 231 (1995) 616–620.
[10] F.-J. Liu, H. Ota, S. Okamoto, S. Suda, Proceedings of the International Conference on Metal Hydrogen Systems, 1996, to be published in the Journal of Alloys and Compounds.
[11] L. Schlapbach, F. Meli, A. Züttel, The Electrochem. Soc. 27 (1994) 102–110.
[12] H. Siegenthaler, in: R. Wiesendanger, H.-J. Güntherodt (Eds.), Scanning Tunneling Microscopy, Springer-Verlag, Berlin, 1992.
[13] R.C. Bhardwaj, A. González-Martin, J.O'M. Bockris, J. Electrochem. Soc. 139 (1992) 1050–1058.
[14] P. Allongue, V. Costa-Kieling, H. Gerischer, J. Electrochem. Soc. 140 (1993) 1009–1018.
[15] D. Chartouni, A. Züttel, Ch. Nützenadel, L. Schlapbach, Journal of Alloys and Compounds, 1997, accepted for publication.
[16] F. Niederhauser private communication, H. Siegenthaler and F. Niederhauser, Institute of Inorganic, Analytical and Physical Chemistry, University of Bern, Switzerland.
[17] Zeng Fang Chen, E. Wang, Electroanalysis 6 (1994) 672–676.
[18] M. Miyamura, T. Sakai, N. Kuriyama, K. Oguro, A. Kato, H. Ishikawa, Electrochemical Society Proceedings 92–5, 179–197, 1992.
[19] Pearson's Handbook of Crystallographic Data for Intermetallic Phases, American Society For Metals, 1985.
[20] K. Yvon, Lazy and Pulverix, Laboratoire de Cristallographie, Université de Genève, 24 Quai Ernest-Ansermet, Genève 4, Switzerland.
[21] J.O. Ström-Olsen, Y. Zhao, D.H. Ryan, J. Less-Common Metals 172–174 (1991) 922–927.
[22] A. Züttel, F. Meli, L. Schlapbach, J. Alloys Comp. 200 (1993) 157–163.
[23] M. Pourbaix, Atlas of Electrochemical Equilibria, National Association of Corrosion Engineers, Cebelor, Brussels, 1974.